

## Optimal Design of an Exterior-Rotor Permanent Magnet Generator for Wind Power Applications

A.A. Abdoos\*, M.E. Moazzen, S.M. Hosseini

Department of Electrical and Computer Engineering, Babol Noshiravani University of Technology, Babol, Iran

**Abstract-** High power permanent magnet synchronous generators (PMSGs) are suitable for wind power applications because of their high efficiency. According to the electromagnetic machine design principles, the main disadvantages of low-speed and high-power generators are large size, heavy weight and high manufacturing cost. The main objective of this paper is to optimize the exterior-rotor PMSG for direct-drive wind turbine applications in order to reduce the generator system cost under design constraints. At first, a multidisciplinary and accurate model is proposed for optimal designing of exterior-rotor permanent magnet wind generator system. Next, the design variables that affect the generator system cost are investigated and specified. Furthermore, the impact of these variables on generator efficiency as one of the main design constraints, are investigated. At last, the unified particle swarm optimization (UPSO) technique is used to optimize the design variables based on the presented analytical model. By comparison the optimal design results of this study with two 500-kW inner-rotor PMSGs and one 15-kW prototype exterior-rotor PM wind generator, it is shown that the proposed method yields an optimal design with lower total volume, lower generator system cost and higher efficiency. Moreover, 3-D finite element analysis is employed to verify the obtained results of the proposed optimal design of 500-kW exterior-rotor PMSG.

**Keyword:** Permanent magnet (PM) synchronous generator, Direct-drive wind turbine, Multidisciplinary analytical design model, Optimal design, Finite element analysis (FEA).

### 1. INTRODUCTION

In recent years, wind energy has attracted a large share of attention and investment because of the low cost of energy production, infinite resources, and eco-friendly characteristics [1]. To generate electricity by wind energy, various kinds of generators have been used and each has advantages and disadvantages on its own. Among all electrical generators, permanent magnet (PM) machines have special features that make them well suited for low speed wind power applications. PM machines have some advantages over electrically excited machines such as higher efficiency and reliability. Because of the removal of the external excitation, the machine reliability improved and the conductor losses are eliminated from the rotor [2, 3]. The radial-flux surface mounted PM machine among the various types of PM machines can be a good choice and effectively utilized in gearless scale wind turbines

because of its simple structure, high reliability and good utilization of active materials. Different interesting studies have been carried out on the optimal design of PM generators [3, 4]. Chen et al. offered an optimal design and conducted experimental tests of an exterior-rotor PM generator which is directly coupled to wind turbines [5]. The main objective of the proposed optimization problem in Ref. [5] is to present a low cost magnetic structure. It has been verified that an exterior-rotor permanent magnet synchronous generators (PMSGs) with a simple structure has a good performance over a wide range of speeds and can operate reliably. Polinder et al. made a comparison between different types of wind power generators in terms of annual energy per cost [6]. It has been shown that the direct-drive PM generator has the highest produced energy, compared to synchronous generators with electrical excitation and doubly-fed induction generators. Optimal design of several PMSGs with different rated powers has been presented in Ref. [7] for a given wind profile. The generated energy is estimated in order to find the most suitable generation system. It is shown that the high power PM generators with lower nominal speed will have better performance in term of the torque per cost and torque density. Potgieter et al. proposed a cost-effective technique to minimize the

Received: 07 Jun. 2020

Revised: 24 Sep. 2020

Accepted: 14 Dec. 2020

\*Corresponding author:

E-mail: a.abdoos@nit.ac.ir (A.A. Abdoos)

DOI: 10.22098/joape.2021.7337.1532

**Research Paper**

© 2021 University of Mohaghegh Ardabili. All rights reserved.

torque ripple of the exterior-rotor PM generator for wind power applications [8]. The voltage quality, load torque ripple, mass and ease of manufacturing are the main limits which have been considered in the optimal design process. In Ref. [9], authors used Lagrange multiplier as a well-known mathematical approach and a simple optimization technique to increase the apparent air-gap power value of a large PMSG under a maximal tangential stress constraint. Alshibani et al. proposed a new method of costing based on a lifetime cycle assessment that adds the cost of subsystems and other components to the PM wind generator lifetime cost and compared the lifetime revenues of the resulting generators [10]. In Ref. [11], an optimal design of the exterior-rotor PM wind generator has been presented to satisfy the required power of generator while minimizing the cogging torque and back electromotive force of total harmonic distribution. In Ref. [12], a 6-MW direct-drive PMSG for offshore wind turbines is optimized to reduce the cost of energy using a pattern search process based on hybrid genetic algorithm. Moreover, four different objective functions have been defined to present an optimal design with low cost of energy. The optimal results show that the surface-mounted PMSG produces lower cost of energy. Puri et al. in Ref. [13], recount the design optimization of inner and exterior-rotor of a PMSG for wind power applications considering the generator weight. The proposed results show that the weight of exterior-rotor generator is lower than inner-rotor type. In Ref. [14], a multiphysics design optimization has been proposed to obtain an optimum cost-effective PMSG for wind power applications. The optimization goal is to minimize the cost by using a well-known deterministic optimization algorithm i.e. sequential quadratic programming. The model considers the generator active materials, power converter cost and losses. Asef et al. offered a dual-level response surface method coupling with Booth's algorithm and also simulated annealing method for design optimization of an exterior-rotor PMSG in order to maximize the output power and minimize the manufacturing cost [15]. In Ref. [16], a mathematical model has been provided for optimal design of a high-efficiency surface-mounted PM synchronous machine. This model is based on PM operating point, embrace and torque angle. These three factors are related to the air-gap size, PM size, efficiency, cogging torque and over load capacity. Then, Maxwell 2D FEM is used to optimize all of the initial design parameter. The gearless PM wind generators are characterized by large diameter, heavy weight and high cost [5, 9] because of low speed operation. Thus, to make wind power competitive with

**Table 1. Main parameters and constants for modeling**

Parameters	Value	
PMSG	500-kW PMSG	15-kW PMSG
Rated output power [kW]	500	15
Rated Line voltage [V]	400	400
Rated shaft speed [rpm]	32	150
Magnetic modeling		
Lamination core	M-19	
$\rho_h$ [W/kg]	2	
$\rho_e$ [W/kg]	0.5	
Economic modeling		
Copper cost [Euro/kg]	15	
NdFeB cost [Euro/kg]	30	
Lamination core cost [Euro/kg]	3	
Reference structure cost [Euro]	15000	
Power electronic cost [Euro/kW]	40	
Electrical subsystem cost [Euro/kW]	38	

other renewable energies, the optimal design of the main components of the wind power system (i.e., generator, power converters and etc.) is crucial. In this study, the cost of generation system is chosen as the main objective function in order to investigate a cost-effective PM wind generator system. For this purpose, a multidisciplinary analytical design model (MADM) of an exterior-rotor PMSG is firstly presented. The MADM has been composed of five models: mechanical, electrical, geometric, magnetic and economic. Next, the design variables that affect the generator system cost and also the system efficiency (as one of the main design constraints) are investigated. Then, the unified particle swarm optimization (UPSO) is used to obtain the optimum value of variables that minimizes the intended objective function. To show the effectiveness of the MADM, the obtained results are compared to optimized inner- and exterior-rotor prototype PM generators. Finally, the analytical optimization results are presented using finite elements analysis software.

## 2. DESIGN SPECIFICATIONS

The PMSG and wind turbine specifications are described in this section. The main generator specifications are listed in Table 1.

### 2.1. Wind turbine

In this study, the direct-drive wind turbine is chosen. In comparison to geared-drive turbine, this type has advantages from several viewpoints such as efficiency, energy, reliability and availability [3, 9]. The rated wind speed in wind site is assumed to be 12 m/s. The rated shaft speed of 500-kW and 15-kW direct-drive wind generator is estimated to be 32 rpm and 150 rpm, respectively.

### 2.2. PMSG

The PMSG which is used for conventional wind

generators, has been designed as an inner-rotor configuration. The rotor diameter of this type is relatively small, so it is difficult to attach multiple magnets on rotor. On the other hand, the PM generator needs a very large pole number to produce normal frequencies at very low speeds. Therefore, to cope with various difficulties of designing a direct-drive wind generator, the exterior-rotor structure is adopted. This topology has advantages in aspects of the efficiency and output power density. Moreover, compared to the inner rotor structure, it can be designed with a multi-pole rotor and thus electric power can be generated at low speeds [5, 11, 13]. The structure of an exterior-rotor PMSG is shown in Figure 1. The following assumptions are made prior to start of the design process of the exterior-rotor PMSG:

- The number of slots per pole and phase ( $q$ ) is 1. The air-gap is set to be 0.001 times the stator exterior diameter ( $D$ ) in order to assure the proper mechanical operation [17]. Also, a two-layer winding is used while the ratio of coil span to pole pitch is set to 5/6 to minimize both 5<sup>th</sup> and 7<sup>th</sup> harmonics.
- The slot space (fill) factor is set to 0.6. To have a suitable slot shape, the ratio between the slot depth ( $h_i$ ) and the slot width ( $w_s$ ) can be limited in the range of 4 to 10 [7].
- In order to prevent the mechanical stress, the tooth width should not be less than 10 mm [18].
- The NdFeB50 is chosen as PM material that its remanence flux density ( $B_r$ ) is 1.42 T.
- Based on the normal frequency range for PM wind generators i.e. 30-80 Hz [5] or 10-70 Hz [19], the required number of generator pole pairs (as one of the optimization variables) is chosen over the range of 19-130 for 500-kW generator and 4-32 for 15-kW generator.
- The minimum efficiency in the optimization process is set to 95%.

### 3. MULTIDISCIPLINARY ANALYTICAL MODEL OF EXTERIOR-ROTOR PMSG

The proposed MADM in this study includes the wind turbine mechanical behavior, the electric and electromagnetic behavior of the generator as well as total construction cost of the machine under study. Therefore, the MADM can be organized by five models: mechanical, electrical, geometrical, magnetic and economic models.

#### 3.1. Mechanic modeling

The aim of this section is to estimate the available

power on the turbine shaft, rotational speed and also

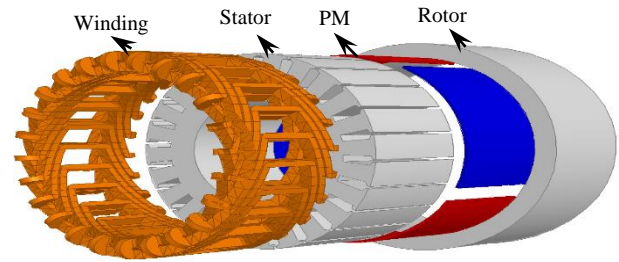


Fig. 1. The construction of exterior- rotor PM machine

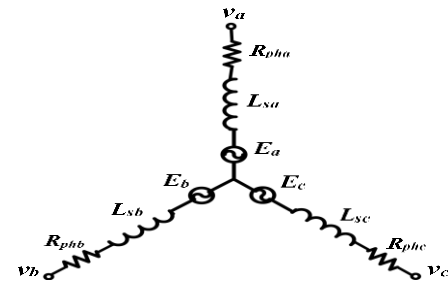


Fig. 2. Three-phase equivalent circuit of the PMSG

friction and windage losses. The available rated shaft power can be expressed as [1, 6, 20]:

$$P_m = 0.5 C_p \rho_{air} \pi R^2 v^3 \tag{1}$$

where,  $C_p$ : aerodynamic efficiency;  $R$ : radius of the turbine blade (m);  $\rho_{air}$ : air density ( $\text{kg/m}^3$ );  $v$ : rated wind speed (m/s)

The rated shaft speed (rev/s) is given by [4, 14]:

$$n_r = \frac{v \lambda}{2\pi L_b} \tag{2}$$

where  $\lambda$  is the tip speed ratio and  $L_b$  is blade length. Due to the low speed operation nature of shaft, mechanical losses in a direct-drive PM wind generator are usually small and so they will not be considered in this study. The total frictional and windage losses at rated speed are considered to be 0.005 times the mechanical shaft power [14].

#### 3.2. Electric modeling

The electrical model describes the electrical behavior of the generator that consists of the equivalent circuit and analytic equations. The model outputs include voltage, current and copper losses. The equivalent circuit of the three-phase PMSG with star connection is shown in Figure 2. The electromotive force (EMF) of the first phase for an  $m$ -phase PMSG with uniformly winding repartition, can be expressed as:

$$\vec{E}_a = \vec{V}_a + R_{pha} \vec{I}_a + j\omega L_{sa} \vec{I}_a \tag{3}$$

where,  $V_a$ : terminal phase voltage (v);  $I_a$ : stator current (A);  $R_{pha}$ : phase resistance ( $\Omega$ );  $L_{sa}$ : synchronous inductance (H);  $\omega$ : angular frequency (rad/s).

The rms value of the stator current at rated load is

given by:

$$I_{rms} = \frac{P_{out}}{3 V_a \cos \phi} \quad (4)$$

where,  $P_{out}$  is the rated output power and  $\cos \phi$  is power factor. Since the copper losses are dependent on the phase current and winding resistance, it can be formulated as [21]:

$$P_{Cu} = m R_{pha} I_{rms}^2 \quad (5)$$

### 3.3. Geometric modeling

Generally, the design of electric machines begins with the sizing equation. To this end, the output power of a radial-flux PMSG can be written in terms of the main dimensions ( $D$  and  $L$ ) of the machine as [9, 21-23]:

$$P_{out} = \frac{1}{k_e} S_g \cos \phi \quad (6)$$

$$S_g = 0.5 \pi^2 k_w n_r D^2 L A_m B_{mg1} \quad (7)$$

In the above equations,  $S_g$  is the apparent power at the air-gap and  $k_e$  is the EMF to terminal voltage.  $k_w$  and  $A_m$  are the winding factor and stator linear current density (or specific electric loading), respectively.  $D$  is the air-gap or stator exterior diameter and  $L$  is the stator length.  $B_{mg1}$  is the maximum value of the fundamental component of the air-gap flux density due to the PMs, that is obtained from Eq. 8 [6]. In this equation,  $B_{mg}$  is the peak value of the air-gap flux density and  $\alpha_i$  is the pole-shoe arc to pole-pitch ratio. In the design process,  $B_{mg}$  can be chosen in the range of 60-80 percent of the remanent flux density of PM [22].

$$B_{mg1} = \frac{4}{\pi} B_{mg} \sin\left(\frac{\pi}{2} \alpha_i\right) \quad (8)$$

The geometrical parameters and dimensions of the exterior-rotor PMSG are shown in Figure 3. If the iron core is assumed to be ideal, the magnet height that provides the required excitation on the air-gap can be written as [6, 7]:

$$h_{pm} = \frac{B_{mg}}{B_r} \mu_{rec} g_{eff} \quad (9)$$

where  $\mu_{rec}$  and  $g_{eff}$  are the PM recoil line relative permeability and effective air-gap length, respectively.

### 3.4. Magnetic modeling

The purpose of this section is to compute the synchronous inductance and the iron losses. The synchronous inductance includes the leakage and magnetizing inductances [6, 22]:

$$L_s = L_l + L_m \quad (10)$$

where  $L_l$  is the leakage inductance, which can be estimated as a sum of three inductances, i.e., slot leakage, end-winding connection leakage, tooth-top leakage and differential leakage inductance. The details

of these leakage inductances can be found in ref. [22].

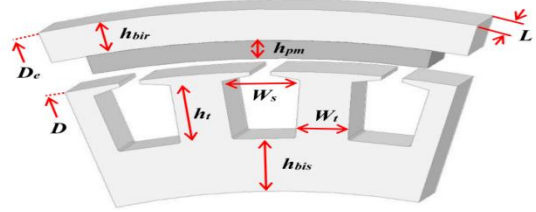


Fig. 3. One pole pitch section of the exterior-rotor PMSG

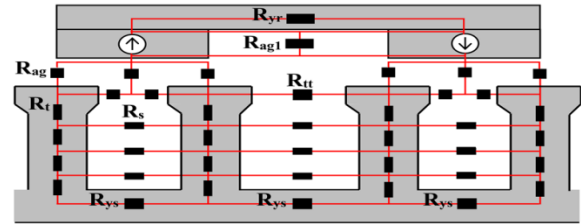


Fig. 4. The proposed reluctance network of exterior-rotor PMSG

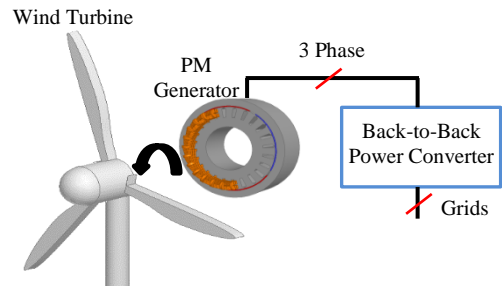


Fig. 5. Configuration of the direct-drive exterior-rotor permanent magnet wind power generation system

In Figure 4, the proposed reluctance network of the exterior-rotor PMSG is shown. The magnetizing inductance of a radial-flux, surface-mounted PMSG is given by [6, 7, 22]:

$$L_m = \mu_o \frac{m D_e}{\pi p^2 g_{eff}} L (N_{ph} k_w) \quad (11)$$

where  $\mu_o$  is the air permeability and  $D_e$  is the stator exterior diameter.  $p$  and  $N_{ph}$  are the number of pole pairs and number of turns per phase, respectively. The specific iron losses in the stator teeth and yoke are approximated with [6, 12]:

$$P_{Fe} = 2 \rho_h \frac{f}{50} \left(\frac{B_{Fe}}{1.5}\right)^2 + 2 \rho_e \left(\frac{f}{50}\right)^2 \left(\frac{B_{Fe}}{1.5}\right)^2 \quad (12)$$

where  $f$  and  $B_{Fe}$  are the frequency of the field and flux density of the stator teeth or yoke, respectively.  $\rho_h$  is the hysteresis specific loss and  $\rho_e$  is the eddy current specific loss (w/kg) at flux density of 1.5 T and frequency of 50 Hz. In order to calculate the total generator iron losses, the specific iron losses in the various parts, i.e., teeth and yoke are multiplied by respective weight and finally must be added together. The laminated core specifications are given in Table 1.

### 3.5. Power converter modeling

The direct-drive permanent magnet wind generator can operate at various wind speed while the maximum efficiency is achieved by connecting to the grid via a back-to-back PWM full power electronic converter. This configuration can be observed in Figure 5. In this section, the power converter loss is calculated and its cost estimation is presented in the next section. There are various ways to calculate the power converter loss. In this study, the power converter losses  $P_{CN}$  is calculated as [4, 6]:

$$P_{PC} = \frac{P_{CN}}{31} \left( 1 + 10 \frac{I_P}{I_{PN}} + 5 \left( \frac{I_P}{I_{PN}} \right)^2 + 10 \frac{I_G}{I_{GN}} + 5 \left( \frac{I_G}{I_{GN}} \right)^2 \right) \quad (13)$$

where PCN is the converter dissipation at the rated load which is considered to be 3% of the rated power. IP is the PMSG side current and IPN is the nominal current of the PMSG side converter. IG is the grid side current and IGN is the nominal current of the grid side converter. The IP and IG are varied according to wind speeds.

### 3.6. Economic modeling

In the economic modeling, three kinds of costs is considered: the generator cost, electrical subsystem cost and the power converters cost. The generator cost is composed of the active material and structure cost. The active material cost is calculated as:

$$C_{mat} = m_{PM} c_{PM} + m_{Cu} c_{Cu} + m_{Fe} c_{Fe} \quad (14)$$

where mpm, mcu and mFe are the PM, copper and iron core weights by their respective the specific cost (cPM, cCu and cFe). The generator structure cost can be approximated as [3, 4, 18]:

$$C_{st} = \frac{c_{str}}{2} \left[ \left( \frac{D_e}{D_{ref}} \right)^3 + \left( \frac{L}{L_{ref}} \right)^3 \right] \quad (15)$$

where cstr is the specific cost of a reference machine structure with 1 m length and 2 m diameter. The power converter (CPC) and electrical subsystem (CSUB) costs can be calculated as a function of the output power. The total generator system cost can be written as [4]:

$$C_T = C_{mat} + C_{st} + C_{PC} + C_{SUB} \quad (16)$$

The values of main parameters and constants which are essential for modeling are given in Table 1.

### 3.7. Design validation

In the generator design process, it should be noted that the main parameters of machine i.e., rated voltage and air-gap flux density must be adjusted according to their nominal values. Moreover, mechanical and electrical constraints based on the generator application must be applied in the design process to improve the machine overall performance. In the proposed analytical design, the terminal voltage regulation is implemented as:

- 1) The induced voltage  $E_a$  is estimated by  $k_e V_a$ .
- 2) The terminal voltage can be calculated based on the equivalent circuit by referring to electric modeling and (3).
- 3) The difference between the calculated terminal voltage and its rated value (i.e. 400 V) is considered to be less than 3%.

The air-gap flux density is calculated as:

1. As one of the design variables, the maximum value of the air-gap flux density Bmg will be estimated by (0.6-0.8) Br.
2. The maximum air-gap flux density can be calculated by referring to the exterior-rotor PMSG reluctance network.
3. The difference between the calculated maximum air-gap flux density and the estimated Bmg should be less than 3%.

### 3.8. The design process

To summarize the design procedure, a flowchart is developed as depicted in Figure 6. Using initial data input, design variables are randomly set by UPSO and the exterior-rotor PMWG will be optimized to obtain the minimum generation system cost. Next, the stator diameter, magnet height and slot dimensions are calculated and then the air-gap flux density is computed based on previously computed parameters. Also, the terminal voltage can be calculated at the rated load using the electrical model of generator.

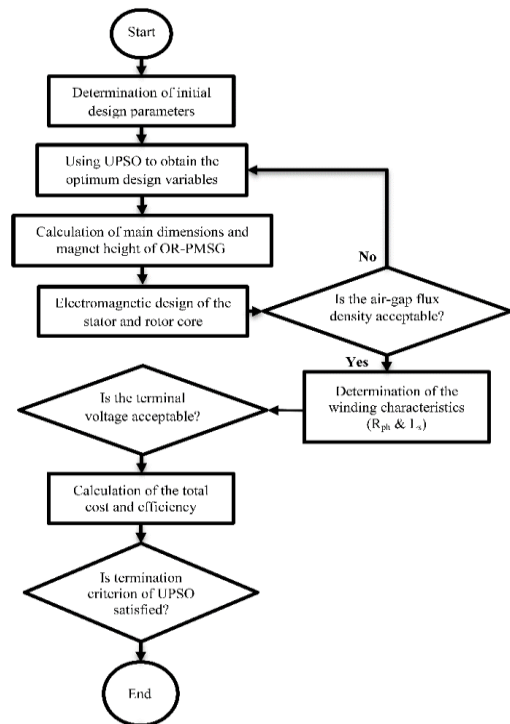


Fig. 6. The flowchart of the optimal design procedure

At last, the total cost and efficiency can be easily obtained. If the UPSO termination criterion is satisfied, the optimal design procedure will stop, else the procedure will repeated in a similar manner.

**4. THE DESIGN VARIABLES**

The design variables are the main parameters of the proposed optimization framework. Therefore, the optimal values of these parameters as well as proper selection of their binderies, are of great importance in the design process. In this section, the impact of design variables on the generator system cost and generator efficiency are investigated. The impact of the specific electric loading ( $A_m$ ) and maximum value of air-gap flux density ( $B_{mg}$ ) together with other effective parameters on the generator system cost are shown in Figures 7 and 8, respectively. Also, the impact of these parameters on generator efficiency is also shown in Figure 9. The design variables and their binderies are:

$$10000 < A_m < 60000 \text{ (A/m)}$$

$$0.6 B_r < B_{mg} < 0.8 B_r \text{ (T)}$$

$$1.1 < B_{mbis} < 1.5 \text{ (T)}$$

$$1.3 < B_{mbir} < 1.6 \text{ (T)}$$

$$1.5 < B_{mt} < 2 \text{ (T)}$$

$$3 < \text{Current density} < 6 \text{ (A/mm}^2\text{)}$$

$$0.6 < \alpha_{PM} < 0.9$$

$$0.14 < k_L < 0.5$$

$$1 < k_e < 1.4$$

$$19 < p < 130$$

It can be seen from Figure 7(a) that decreases in  $A_m$  and  $B_{mg}$  leads in an increase in the generator system cost. According to Figure 7(b), the maximum generator system cost occurs at  $A_m=60$  (KA/m) and  $L/D=0.14$ . It can be seen from Figure 7(c) that when  $A_m=10$  (KA/m) and  $\alpha_i=0.9$ , the minimum cost is obtained. Figure 7(d) shows that when the current density decreases and  $A_m$  increases, the cost is continuously increased. According to Figure 7(e), the minimum cost occurs at the point with  $A_m=60$  (kA/m) and  $k_e = 1$ . It can be seen from Figure 7(f) that decreases in  $A_m$  and pole pairs ( $p$ ), result in a continuous increase in the cost value. According to Figure 7(g), the minimum generator system cost occurs at  $A_m=60$  (kA/m) and  $B_{ys}=1.5$  (T). Referring to Figure 7(h), it can be seen that the cost can decrease by either a decrease in  $A_m$  or an increase in  $B_t$ .

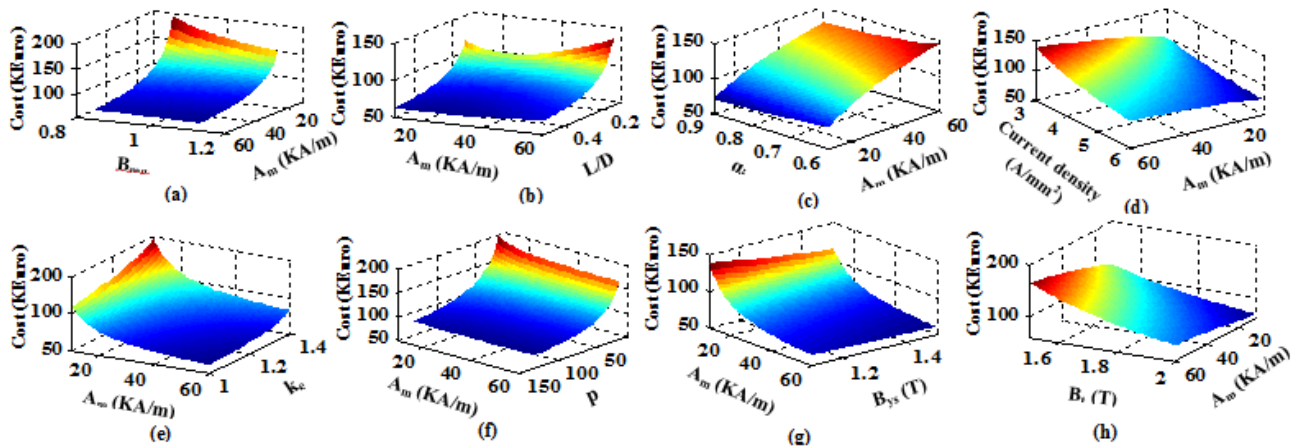


Fig. 7. The impact of  $A_m$  with other design variables on generator system cost

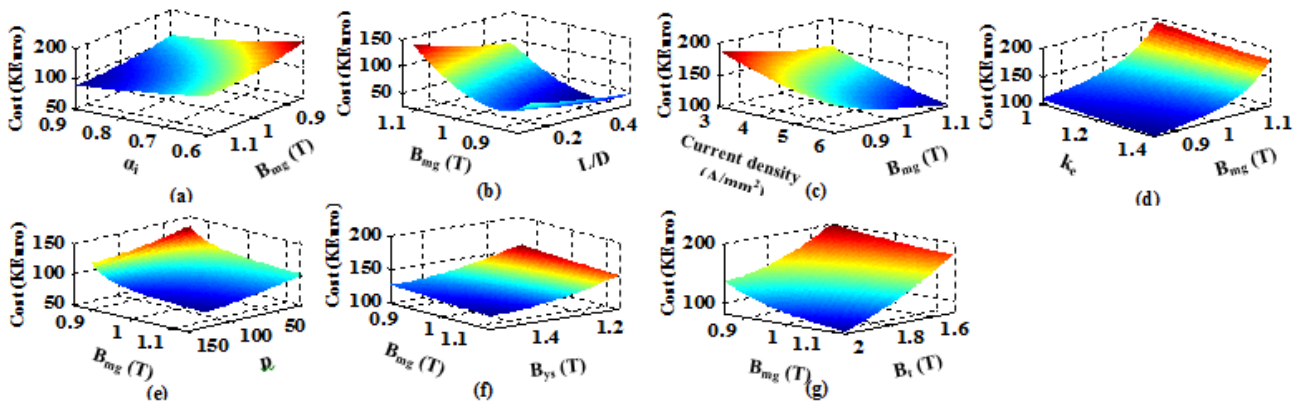


Fig. 8. The impact of  $B_{mg}$  with other design variables on generator system cost

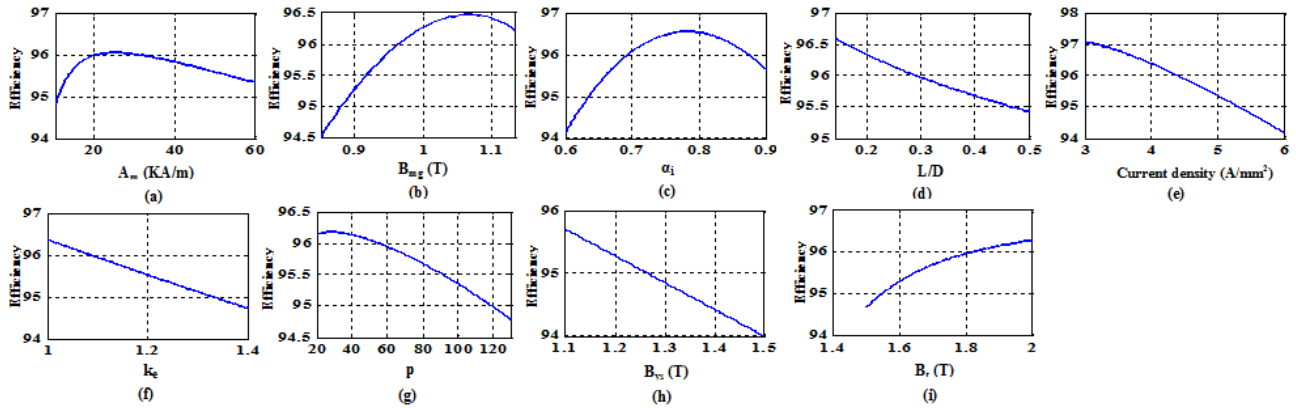


Fig. 9. The impact of design variables on the generator efficiency

Table 2. The design variables and optimization results of 500-kW and 15-kW PMSGs

Parameters	Range		Value		
	Min	Max	500-kW PMSG	15-kW PMSG	
$A_m$ [KA/m]	10	60	59.9	55.16	
$B_{mg}$ [T]	0.852	1.136	1.135	1.02	
L/D	0.14	0.5	0.28	0.16	
$k_e$	1	1.4	1.23	1.07	
$\alpha_i$	0.6	0.9	0.86	0.82	
$p$	500-kW PMSG	19	130	37	-
	15-kW PMSG	4	32	-	18
Current density [ $A/mm^2$ ]	3	6	5.9	5.8	
$B_{ys}$ [T]	1.1	1.5	1.49	1.51	
$B_{yr}$ [T]	1.3	1.6	1.59	1.56	
$B_t$ [T]	1.5	2	1.63	1.51	
Line-to-line $E_{rms}$ [V]			481.57	442.91	

Table 3. Comparison of optimal designs of optimized 500-kW PMSGs

Parameters	This paper	Ref. [3]	Ref. [7]
Main dimensions			
Air-gap diameter D [m]	2	2.15	2.26
Stator length L [m]	0.56	0.55	0.54
Stator slot height $h_s$ [mm]	39.33	64	60
Stator slot width $w_s$ [mm]	9.73	11.7	9.2
Stator tooth width $w_t$ [mm]	18.53	11.1	11.2
Stator yoke height $h_{bis}$ [mm]	21.11	15.9	14.2
Rotor yoke height $h_{bir}$ [mm]	19.79	15.4	14.2
Magnet height $h_{pm}$ [mm]	7.6	6.3	5.8
Performance parameters			
Full load efficiency [%]	95.06	94.2	94.15
Total volume [ $m^3$ ]	1.87	2.05	2.2
Core weight [kg]	1706	1786	1860
Copper weight [kg]	401	779	630
Magnet weight [kg]	131	124	121
Active material weight [kg]	2238	2690	2611
Frequency [Hz]	19.73	26.5	30.9

It is clearly observed from Figure 8(a) that the minimum cost is obtained when  $B_{mg}=1.136$  (T) and  $\alpha_i=0.9$ . As can be seen in Figure 8(b), the minimum cost belongs to  $L/D=0.5$  and  $B_{mg}=0.9$  (T). Figure 8(c) shows that increases in  $B_{mg}$  and current density, causes a decrease in the cost value. It can be seen from Figure 8(d) that the cost value can increase by either an increase in  $B_{mg}$  or a reduction in  $k_e$ . Referring to Figure 8(e), it can be observed that when  $B_{mg}$  and  $p$  increase, the cost value decreases. It can be seen that from Figures 8(f) and 8(g) that by increases in  $B_{mg}$ ,

$B_{ys}$  and  $B_t$ , the cost value decreases. In fact, an increase in the flux density, can decrease both the dimension of iron core and cost value.

Furthermore, the impact of design variables on the efficiency as the most important design constraint, is investigated. Referring to Figure 9(a), the maximum efficiency occurs at around  $A_m=25$  (KA/m). In Figure 9(b), it can be seen that the maximum efficiency is obtained when  $B_{mg}$  is in the range of 1-1.1 (T).

According to Figure 9(c), the efficiency has the maximum value at  $\alpha_i=0.8$ . Moreover, as shown in Figures 7(c) and 8(a), the minimum cost occurs at  $\alpha_i=0.8$ . Figure 9(d), shows that by a decrease in  $L/D$ , the efficiency increases. In Figure 9(e), it can be seen that when current density decreases, the efficiency increases. Whilst it is shown in Figure 7(d) and 8(c) that a decrease in the current density can lead to an increase in the cost value. It can also be seen from Figure 9(f) that when  $k_e$  increases, the efficiency decreases. According to Figure 9(g), the maximum efficiency is obtained around 30 pole pairs. In Figure 9(h), it is shown that by decrease in  $B_{ys}$ , the efficiency decreases. Figure 9(i) shows that when  $B_t$  increases, the efficiency increases while according Figures 7(h) and 8(g) the cost value decreases. In Figures 7-9, it can be clearly observed that specified design variables have direct effect on the generator system cost and efficiency. Therefore, the UPSO is used to employ all of the design variables in the optimization process so that a satisfactory compromise among the design objectives is achieved.

### 5. DESIGN OPTIMIZATION AND DISCUSSION

As described in Section 3, the presented multidisciplinary analytical model is applied for the optimal design of a well-adapted exterior-rotor PM generator connected to the wind turbine. The main purpose of the optimization process is to produce a PM wind generator with minimum system cost. In order to demonstrate the effectiveness of the presented

electromagnetic design and multidisciplinary analytical model, two 500-kW inner-rotor and one 15-kW exterior-rotor PMSG have been chosen for simulation studies. In the first step of the optimization process, appropriate intervals for design variables are set based on the design requirements and machine design limitations. The appropriate interval for design variables are provided in Table 2. The optimal design objective can be expressed as the following function:

$$\text{Minimize } F_{\text{cost}} = C_{\text{mat}} + C_{\text{st}} + C_{\text{PC}} + C_{\text{SUB}} \quad (17)$$

The improvement in the proposed objective function ( $F_{\text{cost}}$ ) during the optimization process is shown in Figures 10(a) and 10(b) for the 500-kW interior-rotor generators and the 15-kW exterior-rotor generator, respectively. As results show, the proposed method is able to converge to the optimal solution in less than 100 iterations for both optimized generators. The optimized values of generator parameters are given in Table 2. To show the effectiveness of the presented multidisciplinary design optimization, comparison results are provided in Table 3 and 4. A detailed comparison between the optimized exterior-rotor PMSG and the optimization results of two 500-kW inner-rotor PMSGs reported by Grauers [3] and Li et al. [7] can be found in Table 3. Moreover, Table 4 provides comparison results between an optimized 15-kW PMSG in this paper and that one studied in [8]. The presented results of the optimized PMSG in Figures 7 and 8 are based on two design variables, but the presented optimal design in this paper considers ten design variables. Therefore, the results obtained from optimization process are slightly different. It can be seen that by an increase in the number of design variables, the optimum value of the objective function is improved. Referring to Eq. (7), it is observed that  $A_m$  and  $B_{mg}$  have a greater impact on manufacturing generator dimensions. Moreover, Figure 7(a) shows that by increases in  $A_m$  and  $B_{mg}$ , the manufacturing cost decreases. This fact is also clearly observed in the optimization results of 500-kW and 15-kW exterior-rotor PMSG given in Table 2.

**Comparison with optimized 500-kW PMSGs studied in [3, 7]:** In Table 3, according to the machine dimensions and performances, it can be seen that there is a good agreement between reported results and those obtained in this study. However, our proposed method yields a more optimal design with lower total volume, lower active material weight, lower total system cost and higher efficiency. Furthermore, the volume decrement is about 184056 cm<sup>3</sup> and 333724 cm<sup>3</sup> in comparison with optimized generators in Refs. [3] and [7], respectively. It means that 452 and 373 kg of active

material is saved compared to [3] and [7], respectively. As can be seen, the copper weight decrement has a greater impact on the total weight of the optimized generator. It is because of the fact that the optimum value of the current density which is found by UPSO is about 6 A/mm<sup>2</sup> while it is about 4 A/mm<sup>2</sup> in Refs. [3] and [7]. Therefore, the copper cross sectional and thereby its weight decreases by an increase in the current density. In comparison to [3] and [7], the iron core weight of the optimized generator in this study decreases about 80-kg and 154-kg, respectively but its PM is slightly heavier, because it has a greater height. On the other hand, the efficiency of the optimized 500-kW PMSG is improved 0.86% and 0.91% as compared to [3] and [7], respectively. These comparisons justify the presented method effectiveness.

**Table 4. Comparison of optimal designs of optimized 15-kW PMSG**

Design parameters	This paper	Ref. [8]
Efficiency	95.11	94.4
Total volume (cm <sup>3</sup> )	25564	33541
Generator outer diameter ( $D_e$ ) (mm)	588.16	653.5
Stator outer diameter ( $D$ ) (mm)	560.67	623
Stator stack length (mm)	94.08	100
Magnet thickness (mm)	4.1	6
Magnet to pole pitch ratio ( $\alpha_g$ )	0.82	0.73
Rated line voltage (V)	400	400
Number of poles	36	40
Frequency (Hz)	45	50
Nominal rotational speed (rpm)	150	150

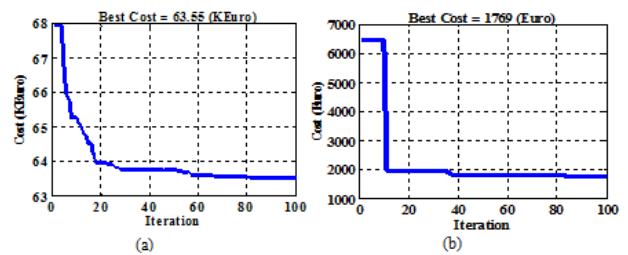


**Fig. 10. The improvement of the objective function ( $F_{\text{cost}}$ ) proposed in this study, (a) 500-kW, (b) 15-kW exterior-rotor PMSG**

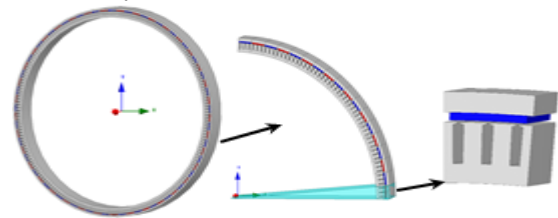


**Fig. 11. The optimized 500-kW ER\_PMSG model in Maxwell software**

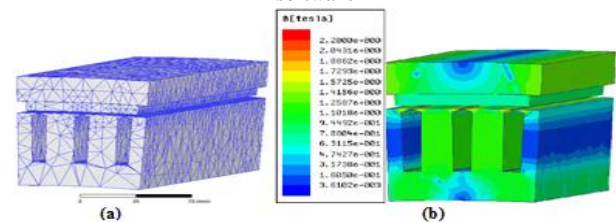


**Fig. 12. (a) Finite element mesh diagram, (b) full-load flux density distribution**

**Table 5. Comparison of obtained results between MADM and FEA for the 500-kW exterior-rotor PMSG**

Generator Parameters	Results		Error (%)
	MADM	FEA	
Line-to-line $E_{rms}$ [V]	481.57	479.16	0.5
$V_L$ [V]	400	398.3	0.42
$B_{mg1}$ [T]	1.41	1.39	2.82
$P_{in}$ [kW]	525.96	526.63	0.13
$T_{in}$ [kN.m]	156.95	157.71	0.48
$P_{out}$ [kW]	500	499.88	0.02
$P_{Fe}$ [kW]	2.63	2.74	4.2
Efficiency [%]	95.06	94.92	0.15
$L_s$ [mH]	1.36	1.32	2.94
$B_{ys}$ [T]	1.49	1.43	4.02
$B_{yr}$ [T]	1.59	1.55	2.51
$B_t$ [T]	1.63	1.58	3.06

**Comparison with an optimized 15-kW PMSG studied in Ref. [8]:** In Table 4, the parameters of the 15-kW PMSG optimized in this study are given and implicitly compared with a prototype exterior-rotor PMSG presented in Ref. [8]. As can be seen, an acceptable agreement does exist with respect to the PMSG performance and dimensions. It can be observed that the total volume of the optimized exterior-rotor PMSG is 7977 cm<sup>3</sup> lower than that of the prototype generator optimized in Ref. [8]. Also, the efficiency of the optimized generator is improved 0.71% compared to the prototype generator. Indeed, a lower total volume as well as a higher efficiency is main advantages of the proposed optimization design.

## 6. FEM ANALYSIS

In this study, the optimal design is found based on the analytical model of the exterior-rotor PMSG. The Ansoft-MAXWELL<sup>®</sup> v.16 software which has been constructed based on the finite element analysis (FEA) method, is employed for simulation studies. Therefore, a 3-D FEA was carried out to verify the optimized 500-kW generator. By making a comparison between the optimized generator parameters obtained from the analytical model and those resulted from FEA, the model accuracy is evaluated. The exterior-rotor PMSG model in Maxwell software is presented in Figure 11. To decrease the solution time, only parts of the generator structure is modeled which reduces the complexity of the simulation. The mesh diagram and flux density distribution for no-load operating conditions are shown in Figures 12(a) and 12(b), respectively. Figure 13(a) shows the waveform of the line-to-line EMF ( $E_{rms}$ ). The fundamental *rms* value of  $E_{rms}$  is 479.16 V with total harmonic distortion (THD) of 9.29%. The waveform of the line-to-line voltages ( $V_L$ ) at full-load operation are shown in Figure 13(b). The fundamental *rms* value of voltage is 398.3 V with THD of 3.87%. It is observed that THD of the induced voltage is higher than the terminal voltage at the rated load, because the generator

winding acts as a low-order filter and thereby high order harmonics have been removed or debilitated. Therefore, the THD of the terminal voltage at rated load has been improved. The mechanical input torque ( $T_{in}$ ) is presented in Figure 13(c). The average mechanical torque is measured 157.71 kN.m. The high torque ripple is due to the space harmonics and cogging torque. The 3-phase instantaneous powers at rated load are shown in Figure 13(d). The average output power is measured 499.88-kW. The air-gap flux density distribution curve at no-load operation is shown in Figure 14(a). The maximum value of the fundamental air-gap flux density  $B_{mg1}$  obtained from the finite element simulation is measured 1.39 T.

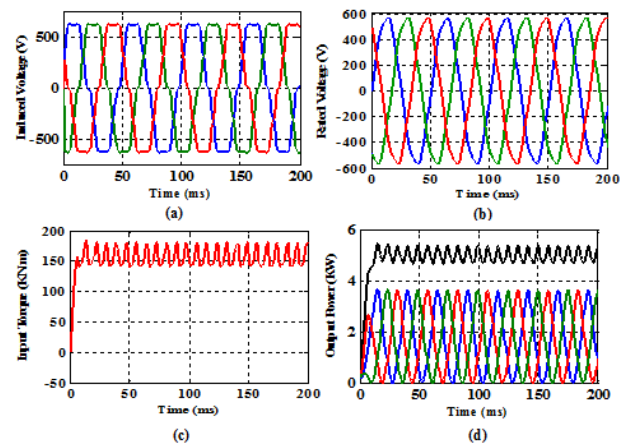


**Fig. 13. (a) The waveform of no-load line-to-line voltages, (b) The waveform of line-to-line voltages at rated load, (c) The waveform of mechanical input torque, (d) The waveform of the output powers at rated load**

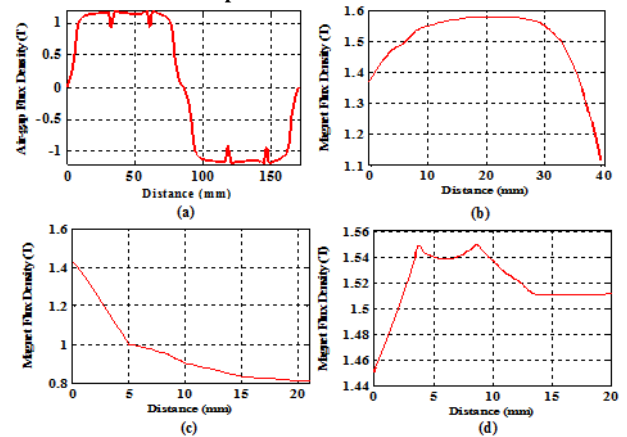


**Fig. 14. (a) Air-gap flux density curve for two pole-pitch, (b) The waveform of magnetic flux variation in the stator tooth, (c) The waveform of magnetic flux variation in the stator yoke, (d) The waveform of magnetic flux variation in the rotor yoke**

The ripple in the air-gap flux density waveform is due to slot opening. The slot opening leads to an increase in the reluctance of magnetic pass and thereby the magnetic flux density decreases. The variation of the magnetic flux density in various parts of the generator i.e. teeth and yokes are shown in Figures 14(b) – 14(d).

The maximum flux density in teeth, stator and rotor yoke are measured 1.58, 1.43 and 1.55 T, respectively. Referring to B-H curve of M-19 lamination core, it is observed that the magnetic saturation in these parts has not occurred. As shown in Table 5, the error is less than 5% and there is a good agreement between FEA and optimal design results.

## 7. CONCLUSION

This paper aims to optimize the exterior-rotor PM wind generators in order to reduce the generation system cost. For this purpose, a multidisciplinary analytical model of the machine was firstly proposed. The proposed MADM includes mechanical, electrical, geometrical, magnetic and economic models. Next, the design variables that affect the generator system cost and also generator efficiency are investigated. Then, the UPSO as an efficient optimization tool are used to obtain an optimum cost-effective PM wind generator. The effectiveness of the proposed MADM has been demonstrated by comparing results obtained from the proposed optimal design with those results related to two optimized 500-kW inner-rotor and one 15-kW exterior-rotor PMSG presented in other works. The comparison results show that the analytical method can yield a PMSG with lower total volume, weight and cost as well as higher efficiency. Finally, the accuracy of optimal design results related to the 500-kW exterior-rotor PMSG is validated through an accurate simulation study using FEA in Maxwell environment.

## Acknowledgement

The authors wish to thank the funding support of Babol Noshirvani University of Technology under grant program numbers BNUT/390066/99 and BNUT/370199/99.

## REFERENCES

- [1] O. Anaya-Lara et al., "Wind energy generation: modelling and control", 1<sup>th</sup> ed., Wiley Press, USA, 2009.
- [2] Y. Chen, P. Pillay and A. Khan, "PM wind generator topologies," *IEEE Trans. Ind. Appl.*, vol. 41, pp. 1619-26, 2005.
- [3] A. Grauers, "Design of direct-driven permanent-magnet generators for wind turbines", *Ph.D. dissertation, Dept. Elect. Comput. Eng., Chalmers Univ. Technol., Goteberg, Sweden*, 1996.
- [4] H. Li and Z. Chen, "Design optimization and site matching of direct-drive permanent magnet wind power generator systems", *J. Renew. Energy*, vol. 34, pp. 1175-84, 2009.
- [5] J. Chen, C. Nayar and L. Xu, "Design and finite-element analysis of an outer-rotor permanent-magnet generator for directly coupled wind turbines", *IEEE Trans. Magn.*, vol. 36, pp. 3802-09, 2000.
- [6] H. Polinder, F. Pijl, G. Vilder and P. Tavner, "Comparison of direct-drive and geared generator concepts for wind turbines", *IEEE Trans. Energy Convers.*, vol. 23, pp. 725-33, 2006.
- [7] H. Li, Z. Chen and H. Polinder, "Optimization of multibrid permanent-magnet wind generator systems", *IEEE Trans. Energy Convers.*, vol. 24, pp. 82-92, 2009.
- [8] J. Potgieter and M. Kamper, "Torque and voltage quality in design optimization of low-cost non-overlap single layer winding permanent magnet wind generator", *IEEE Trans. Ind. Electron.*, vol. 59, pp. 2147-56, 2012.
- [9] J. Tapia et al., "Optimal design of large permanent magnet synchronous generators", *IEEE Trans. Magn.*, vol. 49, pp. 642-50, 2013.
- [10] S. Alshibani, V. Agelidis and R. Duta, "Lifetime cost assessment of permanent magnet synchronous generators for MW level wind turbines", *IEEE Trans. Sustain. Energy*, vol. 5, pp. 10-17, 2014.
- [11] S. Lee, Y. Kim, K. Lee and S. Kim, "Multiobjective optimization design of small-scale wind power generator with outer rotor based on box-behnken design", *IEEE Trans. Appl. Supercond.*, vol. 26, pp. 605-09, 2016.
- [12] A. McDonald and N. Bhuiyan, "On the optimization of generators for offshore direct drive wind turbines", *IEEE Trans. Energy Convers.*, vol. 32, pp. 348-58, 2017.
- [13] V. Puri, Y. Chauhan and N. Singh, "A comparative design study and analysis of inner and outer rotor permanent magnet synchronous machine for power generation in vertical axis wind turbine using GSA and GSA-PSO", *Sustain. Energy Tech. and Assess.*, vol. 23, pp. 136-48, 2017.
- [14] T. Bazzo et al., "Multiphysics design optimization of a permanent magnet synchronous generator", *IEEE Trans. Ind. Electron.*, vol. 64, pp. 9815-23, 2017.
- [15] P. Asef et al., "Multiobjective design optimization using dual-level response surface methodology and booth's algorithm for permanent magnet synchronous generators", *IEEE Trans. Energy Convers.*, vol. 33, pp. 652-9, 2018.
- [16] C. He and T. Wu, "Analysis and design of surface permanent magnet synchronous motor and generator", *CES Trans. Electrical Machines and Systems*, vol. 3, pp. 94-100, 2019.
- [17] J. Pyrhönen, T. Jokinen and V. Hrabovcová, "Design of Rotating Electrical Machines", 1<sup>th</sup> ed., Wiley Press, 2009.
- [18] T. Bazzo et al, "Multidisciplinary design optimization of direct-drive PMSG considering the site wind profile", *Elect. Power Syst. Res.*, vol. 141, pp. 467-75, 2016.
- [19] A. Khan and P. Pillay, "Design of a PM wind, optimized for energy capture over a wide operating range", *Proc. IEEE Int. Conf. Elect. Mach. Drives*, pp. 1501-06, 2005.
- [20] M. Nasiri, J. Milimonfared and S. H. Fathi, "Efficient low-voltage ride-through nonlinear backstepping control strategy for PMSG-Based wind turbine during the grid faults", *J. Oper. Autom. Power Eng.*, vol. 6, pp. 218-28, 2018.
- [21] N. Rostami, "Comprehensive parametric study for design improvement of a low-speed AFPMSG for small scale wind-turbine", *J. Oper. Autom. Power Eng.*, vol. 7, pp. 58-67, 2019.
- [22] J. Gieras, "Permanent magnet motor technology, design and applications", 3<sup>th</sup> ed., Wiley Press, USA, 2010.
- [23] V. Behjat and A. Dehghanzadeh, "Experimental and 3D finite element analysis of a slotless air-cored axial flux PMSG for wind turbine application", *J. Oper. Autom. Power Eng.*, vol. 2, pp. 121-28, 2014.